Solar-Wind Proton Anisotropy Versus Beta Relation

Jungjoon Seough, Peter H. Yoon, Khan-Hyuk Kim, and Dong-Hun Lee

Solar wind proton anisotropy versus beta relation

Jungjoon Seough, Peter H. Yoon[1], Khan-Hyuk Kim, and Dong-Hun Lee
School of Space Research, Kyung Hee University, Yongin, Gyeonggi 446-701, Korea[*]

The present Letter puts forth a possible explanation for the outstanding problem of measured proton temperature anisotropy in the solar wind at 1 AU apparently being regulated by the mirror and oblique fire-hose instabilities. Making use of the fact that the local magnetic field intensity near 1 AU undergoes intermediate-scale temporal variations, the present Letter carries out the quasilinear analysis of the temperature anisotropy-driven instabilities with time-varying local B field, assuming arbitrary initial temperature ratios and parallel betas. It is found that the saturated states in $(\beta_\parallel, T_\perp/T_\parallel)$ space are bounded by the mirror and oblique fire-hose instabilities, which is superficially similar to the observation.

In the present Letter we address an important problem of the proton temperature anisotropy versus plasma beta inverse correlation in the solar wind. The observation of proton temperature anisotropy in the Earth's magnetosheath and in the solar wind near 1 AU [1–9] reveals that the predicted anisotropy does not follow the double-adiabatic theory. In the absence of collisions or significant heat flux, this is commonly interpreted as the result of collective dissipation by kinetic plasma instabilities. For $T_\perp > T_\parallel$, where $T_\perp$ and $T_\parallel$ are perpendicular and parallel proton temperatures defined with respect to the ambient magnetic field, the proton cyclotron, or electromagnetic ion cyclotron (EMIC), and mirror instabilities are excited, while for $T_\perp < T_\parallel$, the unstable fire-hose mode is excited. These instabilities are characterized by the temperature ratio $T_\perp/T_\parallel$ and the plasma beta, $\beta_\parallel = 8\pi n T_\parallel / B^2$, where n and B are density and magnetic field intensity, respectively.

In the literature various empirical marginal stability criteria for these instabilities, known as the anisotropy versus beta relation, have been constructed. For instance, Reference [7] summarizes the various formulas as

$$T_\perp/T_\parallel = 1 + S(\beta_\parallel + \beta_0)^{-\alpha}, \qquad (1)$$

where (S, β_0, α) are given by $(0.43, 0.0004, 0.42)$ for the proton cyclotron, $(0.77, 0.016, 0.76)$ for mirror, $(-0.47, -0.59, 0.53)$ for parallel fire-hose, and $(-1.4, 0.11, 1)$ for the oblique fire-hose instabilities [10, 11]. It is suggested that these relation may be used as closure relations for macroscopic models [12, 13]. It should be emphasized, however, that these relations are not rigorously derived.

In Refs. [14, 15], however, the physics-based inverse correlations were derived for the first time by means of quasilinear kinetic theory. According to Refs. [14, 15] the low-beta regime the anisotropy upper bound should

be regulated by the proton-cyclotron instability, while for high beta's, the upper bound should be governed by the mirror instability threshold. While some observations made in the magnetosheath are consistent with this finding [16, 17], the data obtained in the solar wind at 1 AU, as reported in Refs. [7, 9], for example, are apparently organized according to the mirror mode constraint for all beta regimes in the case of $T_\perp > T_\parallel$, and somewhat less apparently by the oblique fire-hose threshold condition in the case of $T_\perp < T_\parallel$.

In order to resolve this issue, Ref. [18] notes that the asymptotic proton velocity distribution in the saturation stage of the proton-cyclotron instability deviates considerably from the bi-Maxwellian form such that the marginal stability condition may be modified from the linear prediction based upon the bi-Maxwellian model. Alternatively, the presence of Helium ions may substantially raise the proton cyclotron threshold [19, 20]. While these ideas may be relevant, they fail to accurately account for the observational discrepancy.

In the present Letter, we put forth a different explanation. We begin by noting that the solar wind at 1AU is replete with intermediate scale spatio-temporal variations associated with the ambient magnetic field and other physical quantities. An example of the ambient B field intensity variation at 1AU is illustrated in Fig. 1, where the data are taken from the Wind spacecraft measurement made on 29 July 2000. Considering that the average magnetic field shown in Fig. 1 is roughly 8 nT, which translates to local proton gyrofrequency $\Omega_i \simeq 0.77$ (rad/sec), and that the characteristic time scale for the B field variation is ~ 650 sec, which implies $500\,\Omega_i^{-1}$, it is appropriate to treat the B field intensity variation in an adiabatic manner.

Since the proton cyclotron wave relies on the cyclotron resonance $\omega - k_\parallel v_\parallel - \Omega_i(x, t) = 0$, while the mirror mode is dictated by the Landau resonance $\omega - k_\parallel v_\parallel = 0$, we expect that the adiabatic variation of B field may lead to the suppression of the proton-cyclotron instability, while the mirror instability may be largely unaffected. Here, ω, $k_\parallel$, $v_\parallel$ are the wave angular frequency, wave vector and velocity components parallel to $\mathbf{B}$, and $\Omega_i(x, t) = eB(x, t)/m_i c$ corresponds to the locally-varying proton

---
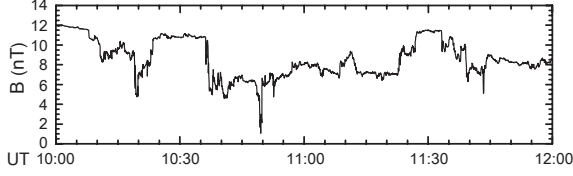
FIG. 1: The local variation of the ambient B field intensity measured by the Wind spacecraft on 29 July 2000 at 1 AU.

cyclotron frequency, e, m_i, and c denoting the unit electric charge, the proton mass, and the speed of light *in vacuo*, respectively.

In order to verify this hypothesis we impose the adiabatically varying local proton gyrofrequency, $\Omega_i \to \Omega_i(t)$ to the basic theory. Note that in general the gyrofrequency should have both the spatial and temporal dependences, $\Omega_i(x, t)$. However, for the sake of simplicity, we consider only the temporal variation in the present Letter. A more general analysis is the subject of the future work. The time-varying gyrofrequency also affects the right-hand circularly polarized kinetic fire-hose resonance condition, $\omega - k_\| v_\| + \Omega_i(t) = 0$, in the case of $T_\perp < T_\|$. Let us assume that the proton velocity distribution function is given by a time-dependent bi-Maxwellian form, $f_i(v_\perp, v_\|, t) = A(t) \exp[-v_\perp^2/\alpha_\perp^2(t) - v_\|^2/\alpha_\|^2(t)]$, where $\alpha_\perp(t) = [2T_\perp(t)/m_i]^{1/2}$, $\alpha_\|(t) = [2T_\|(t)/m_i]^{1/2}$, $A^{-1}(t) = \pi^{3/2}\alpha_\perp^2(t)\alpha_\|(t)$, which is of course, an approximation, but it was demonstrated to be quite adequate in Refs. [14, 15].

The adiabatic time dependence of the local magnetic field intensity is modeled by $B(t) = B_0 \Delta(t)$, where $\Delta(t)$ is to be determined. When $T_\perp/T_\| > 1$, the instantaneous dispersion relations for the proton-cyclotron (denoted with superscript C) and mirror (denoted by M) modes are given, respectively, by [15]

$$\frac{c^2 k^2}{\omega_{pi}^2} = -2\lambda\left(\Lambda_0 - \Lambda_1\right)\left(1 + \frac{T_\perp}{T_\|}\frac{Z'(\xi)}{2}\right), \qquad (2)$$

where $\xi = i\gamma_{\mathbf{k}}^M/k_\| \alpha_\|$, $\lambda = k_\perp^2 \alpha_\perp^2/2\Omega_{i0}^2\Delta^2(t)$, and

$$\frac{c^2 k^2}{\omega_{pi}^2} = -\frac{\omega}{\Omega_i} + \frac{2\Lambda_1}{\lambda}\left[\xi Z(\zeta) - \left(\frac{T_\perp}{T_\|} - 1\right)\frac{Z'(\zeta)}{2}\right], \quad (3)$$

where $\omega = \omega_{\mathbf{k}}^C + i\gamma_{\mathbf{k}}^C$, $\Omega_i = \Omega_{i0}\Delta(t)$, $\xi = \omega/k_\|\alpha_\|$, and $\zeta = (\omega - \Omega_i)/k_\|\alpha_\|$. In the above $\omega_{pi}^2 = 4\pi ne^2/m_i$ is the square of the proton plasma frequency, $\Omega_{i0} = eB_0/m_i c$ is the reference proton cyclotron frequency, $Z(\zeta)$ is the plasma dispersion function, and $\Lambda_n(\lambda) = I_n(\lambda)e^{-\lambda}$, I_n being the modified Bessel function of the first kind of order n.

The time evolution of $T_\perp$ and $T_\|$ is governed by the quasilinear moment kinetic equation, in which the influence of the proton-cyclotron and mirror modes are simul-

taneously taken into account [15],

$$\frac{dnT_\perp}{dt} = -\int d\mathbf{k} \frac{\gamma_{\mathbf{k}}^M |\delta B_{\mathbf{k}}^M|^2}{2\pi}\left(1 + \lambda(\Lambda_0 - \Lambda_1)\frac{\Omega_{i0}^2}{k^2 v_A^2}\right)$$
$$- \int d\mathbf{k} \frac{\gamma_{\mathbf{k}}^C |\delta B_{\mathbf{k}}^C|^2}{4\pi}\left[1 + \frac{\Omega_{i0}^2}{k^2 v_A^2}\left(\frac{\omega_{\mathbf{k}}^C}{\Omega_{i0}\Delta(t)} - \frac{1}{2} + \frac{\Lambda_1}{\lambda}\right)\right],$$
$$\frac{dnT_\|}{dt} = \int d\mathbf{k} \frac{\gamma_{\mathbf{k}}^M |\delta B_{\mathbf{k}}^M|^2}{2\pi}\left(1 + 2\lambda(\Lambda_0 - \Lambda_1)\frac{\Omega_{i0}^2}{k^2 v_A^2}\right)$$
$$+ \int d\mathbf{k} \frac{\gamma_{\mathbf{k}}^C |\delta B_{\mathbf{k}}^C|^2}{4\pi}\left[1 + \frac{2\Omega_{i0}^2}{k^2 v_A^2}\left(\frac{\omega_{\mathbf{k}}^C}{\Omega_{i0}\Delta(t)} - \frac{1}{2} + \frac{\Lambda_1}{\lambda}\right)\right].$$
$$(4)$$

Here, $|\delta B_{\mathbf{k}}^C|^2/(8\pi)$ and $|\delta B_{\mathbf{k}}^M|^2/(8\pi)$ are spectral magnetic wave energy densities associated with the proton-cyclotron and mirror modes, respectively, and they obey the wave kinetic equations, $\partial|\delta B_{\mathbf{k}}^a|^2/\partial t = 2\gamma_{\mathbf{k}}^a |\delta B_{\mathbf{k}}^a|^2$, where $a = M, C$.
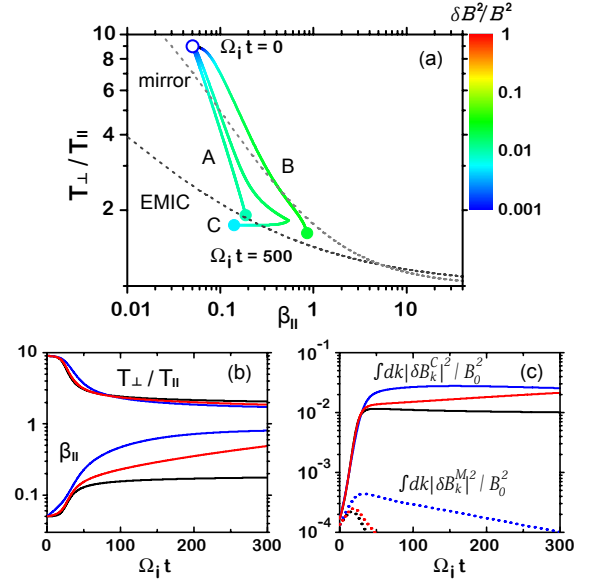
FIG. 2: Sample quasilinear calculations showing (top) the trajectories of initial states in $(\beta_\|, T_\perp/T_\|)$ space, (bottom left) the time evolution of $T_\perp$ and $T_\|$, and (bottom right) the wave spectral energies for proton-cyclotron and mirror modes, for three different time-varying B field models.

Figure 2 shows sample quasilinear calculations of combined mirror and proton cyclotron instabilities under suitable models of the time-dependent magnetic field variation. The trajectories in Fig. 2a shows the time evolution of the the initial state corresponding to $[\beta_\|(0), T_\perp(0)/T_\|(0)] = (0.05, 9)$ in $(\beta_\|, T_\perp/T_\|)$ space. The increase in the total wave energy is depicted by the colormap scale. Case A corresponds to the uniform case, $\Delta(t) = 1$. Next, we modeled the monotonically decreasing field (case B) by $\Delta(t) = 1 - 0.5\tanh(10t/t_*)$, where $\Omega_{i0}t_* = 500$. For B field that is initially decreasing but

subsequently increasing (case C), we choose

$$\Delta(t) = \begin{pmatrix} 1 - t/t_* & 0 \le \Omega_{i0}t \le 200 \\ 3/5 + (t - 200)/t_* & 200 < \Omega_{i0}t \le 500 \end{pmatrix}. \quad (5)$$

For case B, the final state is located in a region intermediate to the proton-cyclotron and mirror instability thresholds, while for case C the final state is located below the marginal proton-cyclotron stability curve. The above three choices of $\Delta(t)$ may be arbitrary, but they are motivated to model the various segments of time-varying B field as shown in Fig. 1.

The time history of the temperature anisotropy and parallel beta is shown in Fig. 2b for case A (black), B (blue), and C (red). Figure 2c plots the evolution of the wave energy densities associated with the proton cyclotron (solid) and mirror (dots) modes. Since the initial state for all three cases correspond to the low-beta regime, the proton cyclotron mode dominates over the mirror mode for all three cases, as dictated by linear theory. However, it is seen that the mirror mode amplitude is appreciably higher for case B when compared with the other two cases.

To complete the analysis, we also consider the case of $T_\perp/T_\parallel < 1$, for which the combined parallel and oblique fire-hose instabilities should be taken into account. However, since the quasilinear theory of oblique fire-hose instability does not yet exist, we confine ourselves only to the parallel fire-hose instability. The instantaneous dispersion relation for the parallel fire-hose mode is given by [14]

$$\frac{c^2 k^2}{\omega_{pi}^2} = \frac{\omega}{\Omega_i} + \left[\xi\, Z(\zeta) - \left(\frac{T_\perp}{T_\parallel} - 1 \right) \frac{Z'(\zeta)}{2} \right], \quad (6)$$

where $\omega = \omega_k^F + i\gamma_k^F$, $\Omega_i = \Omega_{i0}\Delta(t)$, $\xi = \omega/k\alpha_\parallel$, $\zeta = (\omega + \Omega_i)/k\alpha_\parallel$, and the superscript F denotes the parallel fire-hose mode. The time evolution of $T_\perp$ and $T_\parallel$ is governed by the quasilinear moment kinetic equations [14]

$$\frac{dnT_\perp}{dt} = \int dk \frac{\gamma_k^F |\delta B_k^F|^2}{4\pi} \left(\frac{\omega_k^F \Omega_{i0}}{k^2 v_A^2 \Delta(t)} - 1 \right),$$

$$\frac{dnT_\parallel}{dt} = -\int dk \frac{\gamma_k^F |\delta B_k^F|^2}{4\pi} \left(\frac{2\omega_k^F \Omega_{i0}}{k^2 v_A^2 \Delta(t)} - 1 \right), \quad (7)$$

where $|\delta B_k^F|^2/8\pi$ is the spectral magnetic wave energy density associated with the unstable parallel fire-hose mode, which is governed by the wave kinetic equation $\partial |\delta B_k^F|^2/\partial t = 2\gamma_k^F |\delta B_k^F|^2$.

In Fig. 3a we show the trajectories in $(\beta_\parallel, T_\perp/T_\parallel)$ space for three model cases. For all three cases, the initial state is $[\beta_\parallel(0), T_\perp(0)/T_\parallel(0)] = (2, 0.12)$. Case A corresponds to the uniform case, $\Delta(t) = 1$, and the system evolves towards the marginal parallel fire-hose state as expected. For case B we consider the monotonically decreasing B field, modeled by $\Delta(t) = 1 - 0.5\tanh(5t/t_*)$, where $\Omega_{i0}t_* = 1000$. Case C depicts a model where B is
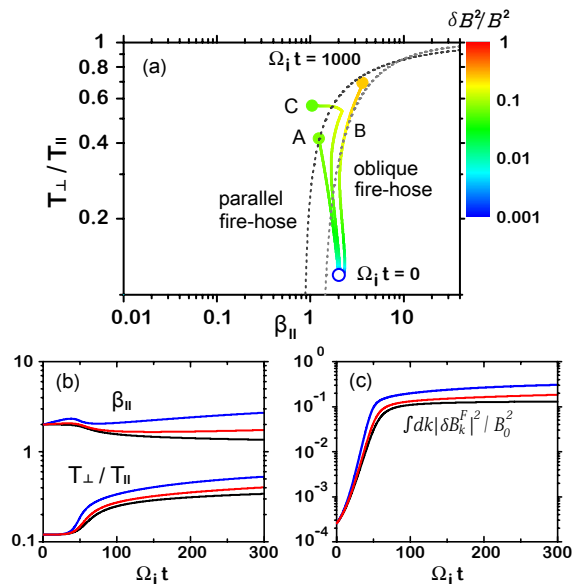
FIG. 3: Sample quasilinear calculations showing (top) the trajectories of initial state in $(\beta_\parallel, T_\perp/T_\parallel)$ space, (bottom left) the time evolution of $T_\perp$ and $T_\parallel$, and (bottom right) the wave spectral energy for parallel fire-hose mode, for three different time-varying B field models.

initially decreasing but subsequently increasing,

$$\Delta(t) = \begin{pmatrix} 1 - 3t/5t_* & 0 \le \Omega_{i0}t \le 500 \\ 7/10 + 3(t - 500)/(5t_*) & 500 < \Omega_{i0}t \le 10^3 \end{pmatrix}, \quad (8)$$

For case B the final state is located in a region intermediate to the parallel and oblique fire-hose instability thresholds, while for case C it is found below the marginal parallel fire-hose curve. Figure 3b depicts the time evolution of $T_\perp/T_\parallel$ and $\beta_\parallel$ for case A (black), B (blue), and C (red). The wave energy density for three cases is shown in Fig. 3c.

On the basis of sample results shown in Figs. 2 and 3, we have considered a number of time-varying B field models, and a large ensemble of initial points in $(\beta_\parallel, T_\perp/T_\parallel)$ space. The basic functional forms of $\Delta(t)$ for increasing and decreasing time profile are variously modeled with the similar forms as described above. Also, we varied the numerical coefficients. We then allowed the initial ensemble points to evolve subject to proton-cyclotron, mirror, and parallel fire-hose instabilities. In order to simplify the analysis, we have adopted the approach that the initial ensemble of solar wind conditions are in arbitrary unstable states. This of course is a idealization of the actual situation, where in reality the solar wind anisotropy must be allowed to develop self-consistently. Upon incorporating the adiabatic spatial dependence of the present model and allowing slow compression or expansion, we may be able to self-consistently generate the anisotropy instead of assuming arbitrary initially anisotropic states. However, such a task is beyond
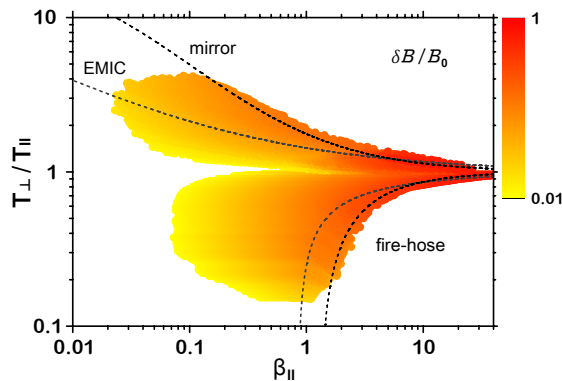
FIG. 4: An ensemble of final states in $(\beta_{\parallel}, T_{\perp}/T_{\parallel})$ space, where the final computation time for all the ensemble points are chosen as $\Omega_i t = 500$ (for initial $T_{\perp} > T_{\parallel}$ cases) and $\Omega_i t = 1000$ (for initial $T_{\parallel} > T_{\perp}$ cases), respectively. The arbitrary initial states were allowed to evolve subject to various instabilities, and for a number of time-varying B field models. After computing quasilinear equations up to $\Omega_i t = 500$ or $\Omega_i t = 1000$ time steps, the final states are plotted above. The colormap depicts the final values of $\delta B/B_0$ in logarithmic scale. Note that we superposed the empirical threshold conditions (1) for a visual comparison.

the scope of the present Letter since we do not yet have the spatial dependence in our model. In any case, adopting the present approach, we have obtained the simulated solar wind proton distribution in $(\beta_{\parallel}, T_{\perp}/T_{\parallel})$ space. The result is shown in Fig. 4. As one can see, the proton data are spread over the region bounded by the mirror (for $T_{\perp}/T_{\parallel} > 1$) and the oblique fire-hose (for $T_{\perp}/T_{\parallel} < 1$) instability thresholds, even though oblique fire-hose instability is not even considered in our model. Note also that a large portion of ensemble points are found below

the proton-cyclotron and parallel fire-hose marginal stability curves. Note that the amplitude of the magnetic fluctuation increases with increasing $\beta_{\parallel}$, especially and along the mirror and oblique fire-hose marginal instability curves. Figure 4 shows a superficial but remarkable resemblance to actual solar wind observations near 1 AU – see, e.g., the second panel of Fig. 1 of Ref. [9].

In summary, we have demonstrated that by judiciously modeling the time-varying B field intensity and by considering an ensemble of initially unstable data points, we may simulate the solar wind proton distribution in $(\beta_{\parallel}, T_{\perp}/T_{\parallel})$ space that qualitatively resembles the actual data in which the marginal mirror-mode and oblique fire-hose mode threshold conditions apparently constrain the proton temperature anisotropy upper bound. The major finding of the present Letter is summarized by Figure 4.

To reiterate, in the real solar wind the temperature anisotropy must be self-generated instead of being imposed as an arbitrary initial condition. This is, in principle, possible once we incorporate the spatial dependence in our model. Also, the effects of density variation can be important. For $T_{\perp}/T_{\parallel} < 1$, the influence of the oblique fire-hose mode, which we ignored in the analysis, should also be included. These are subjects of the future research. The importance of the present work is that the concept of intermediate scale variation of macroscopic quantities such as the B field is a viable one, and that a more rigorous and complete model of the kinetic-global solar wind model may be constructed on the basis of the present method.

[1] B. J. Anderson and S. A. Fuselier, J. Geophys. Res. **98**, 1416 (1993).
[2] S. A. Fuselier, B. J. Anderson, S. P. Gary, and R. E. Denton, J. Geophys. Res. **99**, 14931 (1994).
[3] L. C. Tan, S. F. Fung, R. L. Kessel, S.-H. Chen, J. L. Green, and T. E. Eastman, Geophys. Res. Lett. **25**, 587 (1998).
[4] S. P. Gary, R. M. Skoug, J. T. Steinberg, and C. W. Smith, Geophys. Res. Lett. **28**, 2759 (2001).
[5] J. C. Kasper, A. J. Lazarus, and S. P. Gary, Geophys. Res. Lett. **29**, 1839 (2002).
[6] E. Marsch, X.-Z. Ao, and C.-Y. Tu, J. Geophys. Res. **109**, A04102 (2004).
[7] P. Hellinger, P. Trávníček, J. C. Kasper, and A. J. Lazarus, Geophys. Res. Lett. **33**, L09101 (2006).
[8] L. Matteini, S. Landi, P. Hellinger, F. Pantellini, M. Maksimovic, M. Velli, B. E. Goldstein, and E. Marsch, Geophys. Res. Lett. **34**, L20105 (2007).
[9] S. D. Bale, J. C. Kasper, G. G. Howes, E. Quataert, C. Salem, and D. Sundkvist, Phys. Rev. Lett. **103**, 211101 (2009).
[10] P. H. Yoon, C. S. Wu, and A. S. de Assis, Phys. Fluids B **5**, 1971 (1993).
[11] P. Hellinger and H. Matsumoto, J. Geophys. Res. **105**, 10519 (2000).
[12] R. E. Denton, B. J. Anderson, S. P. Gary, and S. A. Fuserlier, J. Geophys. Res. **99**, 11225 (1994).
[13] P. Hellinger and P. Travnicek, J. Geophys. Res. **113**, A10109 (2008).
[14] J. Seough and P. H. Yoon, J. Geophys. Res. **117**, A08101 (2012).
[15] P. H. Yoon and J. Seough, J. Geophys. Res. **117**, A08102 (2012).
[16] S. P. Gary, S. A. Fuselier, and B. J. Anderson, J. Geophys. Res. **98**, 1481 (1993).
[17] C. Lacombe and G. Belmont, Adv. Space Res. **15**, (8/9)329 (1995).
[18] P. A. Isenberg, Phys. Plasmas **19**, 032116 (2012).
[19] L. Matteini, P. Hellinger, S. Landi, P. M. Travnicek, and M. Velli, Space Sci. Rev., DOI 10.1007/s11213-011-9774-z (2011).
[20] B. A. Maruca, J. C. Kasper, and S. P. Gary **ApJ**, 748,

137 (2012).